Monthly Notices
of the
ROYAL ASTRONOMICAL SOCIETY

Mon. Not. R. Astron. Soc. **420,** 75–83 (2012) doi:10.1111/j.1365-2966.2011.19999.x

# Optical spectroscopy of the quiescent counterpart to EXO 0748−676: a black widow scenario?

E. M. Ratti,[1⋆] D. T. H. Steeghs,[2,3] P. G. Jonker,[1,2,4] M. A. P. Torres,[1,2] C. G. Bassa[5] and F. Verbunt[1,6]

[1]*SRON, Netherlands Institute for Space Research, Sorbonnelaan 2, 3584 CA, Utrecht, the Netherlands*
[2]*Harvard–Smithsonian Center for Astrophysics, 60 Garden Street, Cambridge, MA 02138, USA*
[3]*Department of Physics, University of Warwick, Coventry CV4 7AL*
[4]*Department of Astrophysics, IMAPP, Radboud University Nijmegen, Heyendaalseweg 135, 6525 AJ, Nijmegen, the Netherlands*
[5]*Jodrell Bank Centre for Astrophysics, The University of Manchester, Manchester M13 9PL*
[6]*Astronomical Institute, Utrecht University, PO Box 80 000, 3508 TA Utrecht, the Netherlands*

Accepted 2011 October 12. Received 2011 October 11; in original form 2011 August 2

## ABSTRACT

We present phase-resolved optical spectroscopy of the counterpart to the neutron star (NS) low-mass X-ray binary EXO 0748−676, almost one year after it turned into quiescence. The spectra display prominent H$\beta$ and H$\gamma$ and weak Fe II lines in emission. An average of all the spectra (corrected for the orbital motion) also exhibits a very weak line from Mg I. Tomographic reconstructions show that the accretion disc is not contributing to the optical line emission, which is instead dominated by the irradiated hemisphere of the companion star facing the NS. We could not detect absorption features from the mass donor star in the spectra. The emission lines appear broad, with an intrinsic full width at half-maximum (FWHM) of $255 \pm 22$ km s$^{-1}$. Under the assumption that the width of the Fe II emission lines is dominated by rotational broadening, we obtain a lower limit on the compact object mass which is inconsistent with an NS accretor. We discuss this incongruity and conclude that either the lines are blends of unresolved features (although this requires some fine-tuning) or they are broadened by additional effects such as bulk gas motion in an outflow. The fact that the Fe II lines slightly lag in phase with respect to the companion star can be understood as outflowing gas consistent with a black-widow-like scenario. Nevertheless, we cannot rule out the possibility that blends of various emission lines cause the apparent phase lag of the Fe II emission lines as well as their large width.

**Key words:** accretion, accretion discs – binaries eclipsing – stars: individual (EXO 0748−676) – X-rays: binaries – X-rays: individual: EXO 0748−676.

## 1 INTRODUCTION

EXO 0748−676 was discovered with the *European X-Ray Observatory Satellite* (*EXOSAT*; Parmar et al. 1985) in 1985. Soon after the discovery, the detection of type I X-ray bursts from the source (Gottwald et al. 1986) marked it as a Galactic low-mass X-ray binary (LMXB) where a neutron star (NS) is accreting matter from a low-mass companion star. Many LMXBs are known to be transient, alternating periods of quiescence at a relatively low X-ray luminosity ($\sim 10^{32}$ erg s$^{-1}$ in a 0.5–10 keV range) with month-to-year-long bright X-ray outbursts ($10^{36}$–$10^{38}$ erg s$^{-1}$). EXO 0748−676 has been continuously in outburst for the 24 years since its discovery: tens-of-years-long X-ray outbursts have been observed from a number of LMXBs, e.g. KS 1731−260 (Wijnands et al. 2001), GRS 1915+105 and 4U 1755−338 (see Remillard & McClintock 2006 for a review). During outbursts, mass accretion proceeds at a high rate forming an extended accretion disc around the accreting compact object. X-rays are emitted from the innermost regions, whereas the optical originates further out in the disc. In LMXBs, the disc dominates the optical flux during outbursts, outshining the low-mass companion star. The latter can become visible during quiescence, when the disc is less bright.

A few LMXBs are known where the NS is detected as a pulsar (Chakrabarty 2005) but for the majority of them the companion star is the only viable source of information regarding the system dynamics. Optical spectroscopy of the companion star can be used to measure the orbital parameters and, under certain conditions (see below), the mass of the accreting compact object. This measure is interesting in LMXBs since the accretion process can significantly

⋆E-mail: e.m.ratti@sron.nl

increase the mass of an NS: the maximum mass that an NS can reach is one of the parameters that can distinguish among the existing models for the equation of state (EOS) of those objects (Lattimer & Prakash 2001). The determination of the NS EOS is one of the key goals in the study of NSs and will have strong implication for both astronomy and super-nuclear density matter physics.

The mass of an NS (or a black hole, BH) in a non-pulsating LMXB can be measured by solving the system mass function

$$f(M_D) = \frac{{M_X}^3 \sin^3 i}{(M_D + M_X)^2} = M_X \frac{\sin^3 i}{(1+q)^2} = \frac{P {K_D}^3}{2\pi G}, \quad (1)$$

where $G$ is the universal constant of gravity, $M_D$ and $M_X$ are the masses of the companion and NS, respectively, $P$ is the orbital period, $i$ is the inclination of the orbital plane, $K_D$ is the amplitude of the radial velocity curve of the companion where we define $q \equiv M_D/M_X$. This equation is valid provided that $K_D$ represents the motion of the centre of mass of the companion. Because $f(M_D) \leq M_X$, the mass function provides a lower limit to the mass of the neutron star (Charles & Coe 2006).

Here, $P$ and $K_D$ can be inferred from the orbital Doppler shift of stellar absorption lines originating in the atmosphere of the companion star, which can be visible in the optical spectra during quiescence. $f(M_D)$ can be solved for $M_X$ in eclipsing quiescent LMXBs (van Paradijs & McClintock 1995), where $q$ can be expressed as a function of $K_D$ and the projected rotational velocity of the companion star $v \sin i = [(2\pi)/P)]R_D \sin i$ (Wade & Horne 1988) measured from the broadening of the companion stellar absorption lines (Gray 1992). From $q$ and the eclipse duration, $i$ can be obtained.[1]

The LMXB EXO 0748−676 shows X-ray eclipses (Parmar et al. 1986) and, after a more than 20-yr-long outburst, it turned into quiescence in 2008 September (Torres et al. 2008; Wolff et al. 2008a; Wolff, Ray & Wood 2008b; Hynes & Jones 2009). The optical counterpart to the X-ray source was first found by Parmar et al. (1985) and confirmed by the *Chandra* localization of EXO 0748−676 at RA = $07^{\rm h}48^{\rm m}33\overset{\rm s}{.}73$ and Dec. = $-67^\circ45'07\overset{''}{.}9$ (Torres et al. 2008). A search on photographic plates showed that the source was not detected down to ∼23 mag when the X-ray emission was off. Spectroscopic observations in the optical during the outburst have been performed by Pearson et al. (2006) and Muñoz-Darias et al. (2009), attempting to get a lower limit on the NS mass from He, C and N emission lines probably originating from the inner, heated face of the companion star. The first spectroscopic study of EXO 0748−676 in quiescence was performed by Bassa et al. (2009) two months after the end of the outburst. The spectra, acquired in a 5750–7310 Å wavelength range, were dominated by strong H$\alpha$ and weaker He emission lines coming from the companion star facing the NS, an indication of irradiation. A weak contribution to the lines was due to optical radiation from a residual accretion disc. No absorption lines were detected, preventing a straightforward solution of $f(M_D)$. Nevertheless, the authors could put a lower limit on $K_D$ and the NS mass, $M_{\rm NS} > 1.27\,{\rm M}_\odot$.

Bassa et al. (2009) determined a minimum temperature for the irradiated companion star of EXO 0748−676 of ∼5000 K, the surface temperature of a G-type star. We have performed phase-resolved spectroscopic observations of the optical counterpart to EXO 0748−676 after almost 1 yr of quiescence. We attempted to detect absorption lines from the heated companion star by collecting our spectra in the wavelength range (4222–5701 Å) where a G as well as a K-type star would show absorption lines. We here report on the results of this study.

[1] $\sin^2 i \cos^2(\pi\Delta\phi) = 1 - [\frac{0.49q^{2/3}}{0.6q^{2/3}+ln(1+q^{1/3})}]^2$, where $\Delta\phi$ is the eclipse duration (see Horne 1985). This relation is valid under the assumption that the companion is Roche lobe filling, which holds for LMXBs.

## 2 OBSERVATIONS AND DATA REDUCTION

We performed long-slit phase-resolved spectroscopy of the optical counterpart to EXO 0748−676 with the FOcal Reducer and low dispersion Spectograph (FORS) instrument on the Very Large Telescope (VLT)[2] (grism 1200g+96 and a 1.0 arcsec slit). The orbit was sampled with a total of seventy-three 900-s-long exposures collected between 2010 January 18 [MJD (UTC) = 55214] and 2010 January 22, in the wavelength range 4222–5701 Å. We also acquired template spectra from main sequence G type stars (G5V, G9V and G6V). The seeing across the four nights was between ∼0.8 and ∼1.2 arcsec. The detectors were read out with a 2 × 2 binning, providing a resolution of 2 Å (measured from the width of both arc lines and the night sky O I line at 5577.338 Å) sampled with a dispersion of 0.73 Å pixel$^{-1}$. The images were corrected for bias, flat-fielded and extracted using the FIGARO package within the STARLINK software and the packages PAMELA and MOLLY developed by T. Marsh. We used dome flats for the flat-fielding and we subtracted the sky continuum by fitting clean sky regions along the slit with a second-order polynomial. The spectra were optimally extracted following the algorithm of Horne (1986) implemented in PAMELA and wavelength-calibrated in MOLLY with a final accuracy of 0.1 Å, using arc exposures taken during daytime. The wavelength calibration was corrected for shifts in the single observation with respect to the position of the sky O I line at 5577.338 Å (Osterbrock et al. 1996). Each spectrum has been normalized dividing by a first-order polynomial fit of the continuum. The spectra have been phase binned with $T_0 = 54776.501663 \pm 0.000068$ MJD/TDB from Bassa et al. (2009), which is the closest in time to our observations and with the orbital period $P_{\rm orb} = 0.15933783446$ d from Wolff et al. (2009).

We also analysed sixteen 6-s-long $g'$-band acquisition images, corrected for bias and flat-fielded with standard routines running in MIDAS. The photometry was performed through point spread function fitting, using DAOPHOT II (Stetson 1987). Absolute photometric calibration was not possible due to the lack of observations of $g'$-band standard stars, but a light curve (Fig. 1) of the optical counterpart to EXO 0748−676 was obtained through relative photometry with respect to the reference star USNO-B1.0 0222−0189796. The instrumental magnitude of the reference star was measured with an accuracy of 0.03–0.08 mag across the various images. Relative photometry with respect to two other bright targets has shown that the reference star was not variable during our observations. The light curve was phase folded with the same ephemeris used to phase bin the spectra (see above).

## 3 ANALYSIS AND RESULTS

### 3.1 Individual and trailed spectra

The sole features detected in the individual spectra are the Balmer lines H$\beta$ (4861.327 Å) and H$\gamma$ (4340.465 Å), which are observed as strong emission features. We searched for absorption lines in the individual spectra by cross-correlating with template star spectra, but we found no correlation.

[2] VLT observing program 085.D-0441(C)

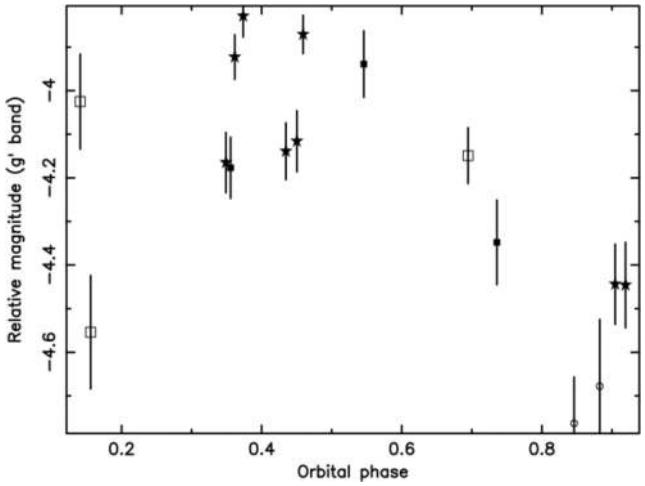


**Figure 1.** $g'$-band light curve determined from the acquisition images. The magnitudes are relative to the bright star USNO-B1.0 0222−0189796. Different symbols refer to different observing nights starting from the night of 2010 January 18 and 19. In temporal order, the observations of the first to the fourth nights are indicated by black stars, black squares, empty circles and empty squares, respectively.

As shown in Fig. 2, more emission features become observable when trailed spectra are constructed. Besides the *s*-waves associated with the Balmer lines, three weak *s*-waves are visible in the region between 4900–5300 Å: the position of the first two lines is consistent with a couple of He I lines, at 4921.929 and 5015.675 Å, but also with Fe lI lines at 4923.92 and 5018.44 Å. No He I line matches the position of the third line, which instead can be Fe II at 5169.03 Å (Moore 1972). This favours an interpretation of the three lines as an Fe triplet as all the three lines are part of multiplet 42.

The variations show only one peak along the orbit. The emission lines fade away and disappear between phases ∼0.75 and ∼0.25, consistent with an emission region located on the inner face of the companion star. There is no indication of absorption lines in the trailed spectra.

### 3.2 Radial velocity of the Balmer lines

For the H$\beta$ and H$\gamma$ lines we have obtained radial velocity curves (see Fig. 3) by fitting single Gaussians to those lines in each 900-s spectrum, including only significant detections on a 3$\sigma$ level. The fitted parameters were normalization, full width at half-maximum (FWHM) and velocity offset of the centroid with respect to the rest-frame line wavelength. The 0.1-Å 1$\sigma$ uncertainty on the velocity offsets due to the wavelength calibration has been added in quadrature to the error on the centroid from the Gaussian fit of each observation. We fitted the radial velocity curve (velocity offset versus phase) for each line with a circular orbit in the form $v(\phi) = \gamma + K_{\rm em}\sin(2\pi\phi+\varphi)$. We measured $\gamma = 54.5 \pm 5.9\,{\rm km\,s^{-1}}$, $K_{\rm em} = 306.1 \pm 5.0\,{\rm km\,s^{-1}}$ and $\varphi = 0.007 \pm 0.004$ from H$\beta$, $\gamma = 32.8 \pm 9.7\,{\rm km\,s^{-1}}$, $K_{\rm em} = 312.6 \pm 6.4\,{\rm km\,s^{-1}}$ and $\varphi = 0.001 \pm 0.007$ from the H$\gamma$ line. The errors are obtained after we artificially increased the error bars on the individual measurements such that the fit reduced $\chi^2$ was 1. The initial reduced $\chi^2$ was 1.6 for the H$\beta$ line (45 degrees of freedom, d.o.f.) and 2.2 for the H$\gamma$ one (33 d.o.f). The fit of the radial velocity curve of the two Balmer lines provides values consistent within 1$\sigma$ for $\varphi$ and $K_{\rm em}$, and within 2$\sigma$ for $\gamma$. The latter is expected to be the same for all the lines, being the radial velocity of the system centre of mass. Note that $\varphi$ and $K_{\rm em}$ instead are not a priori the same for different emission lines, as they could originate from different parts of the irradiated companion star, or in fact regions in the binary.

### 3.3 Averaged spectrum

In order to measure the FWHM of the emission lines, we averaged the spectra in the frame of the companion star. We assumed a circular orbit, shifting the lines by $v = -K_{\rm em}\sin(2\pi\phi+\varphi)$, with $\varphi = 0$. We did not adopt a priori $K_{\rm em}$ obtained from the radial velocity curves of the Balmer lines, since that could be affected by e.g. asymmetry or variations in the line profile from the individual spectra (as for H$\alpha$; Bassa et al. 2009). Moreover, the Balmer lines could originate in a different area than the weaker Fe II lines and thus have a different $K_{\rm em}$. Instead, we proceeded as follows.

(i) We assumed a range of possible values of $K_{\rm em}$ ($200 < K_D < 400\,{\rm km\,s^{-1}}$ in steps of $10\,{\rm km\,s^{-1}}$). For each $K_{\rm em}$ value, we applied

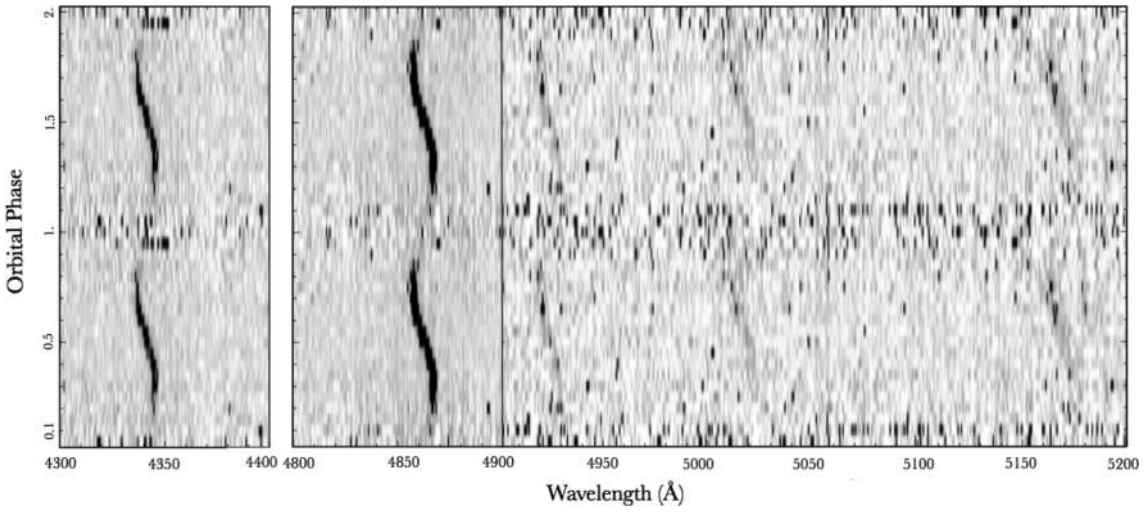


**Figure 2.** Trailed spectra composed by 73 single spectra of the counterpart to EXO 0748−676, phase binned in 20 bins. The two prominent *s*-waves are from the H$\gamma$ and H$\beta$ lines. Three weak lines consistent with Fe II are just visible between 4900 and 5200 Å (see Section 3.1).

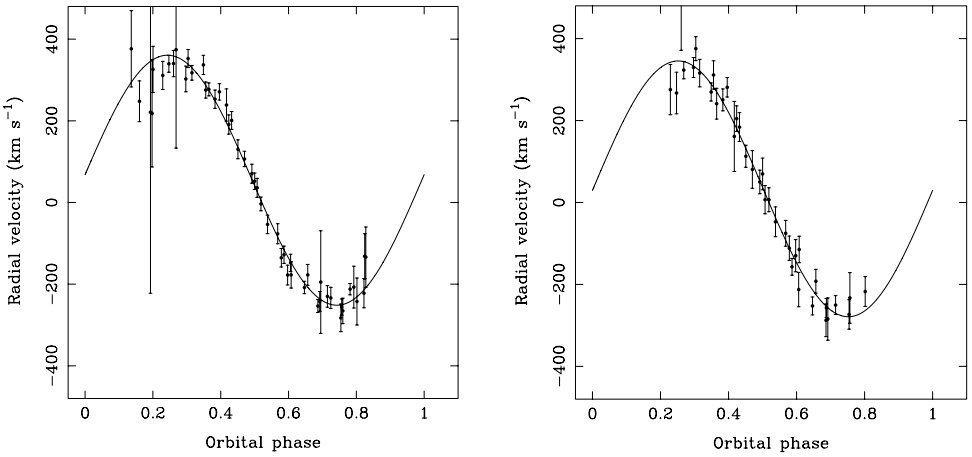


**Figure 3.** Radial velocity curves of the H$\beta$ (a) and H$\gamma$ (b) emission lines. The data points are obtained by fitting a Gaussian to each Balmer line in individual 900-s-long spectra and selecting significant line detections at a 3$\sigma$ level. The solid lines show the best fit to the data.

the circular orbital shift and averaged the spectra between phases 0.3 and 0.7 (the range where the weaker emission lines are clearly detected).

(ii) We measured the FWHM of the emission lines in the averaged spectra, fitting a Gaussian function to each line (see Section 3.1). An orbital shift close to the real one will result in narrower lines in the averaged spectrum.

(iii) We found the $K_{\rm em}$ that results in the narrowest lines: for each line, we plotted the width measured from each average spectrum against $K_{\rm em}$ of the corresponding orbital shift. The uncertainty on the width was large with respect to its variation among different values of $K_{\rm em}$. None the less, each line displays a trend indicating a minimum width at $K_{\rm em} \sim 300\,{\rm km\,s^{-1}}$. The result is consistent with that from the radial velocity curves in Section 3.2.

The spectrum in Fig. 4 is the average of individual exposures comprised between phases 0.35 and 0.7 (where all the emission lines are visible) for $K_{\rm em} = 300\,{\rm km\,s^{-1}}$. Together with H$\beta$ and H$\gamma$,

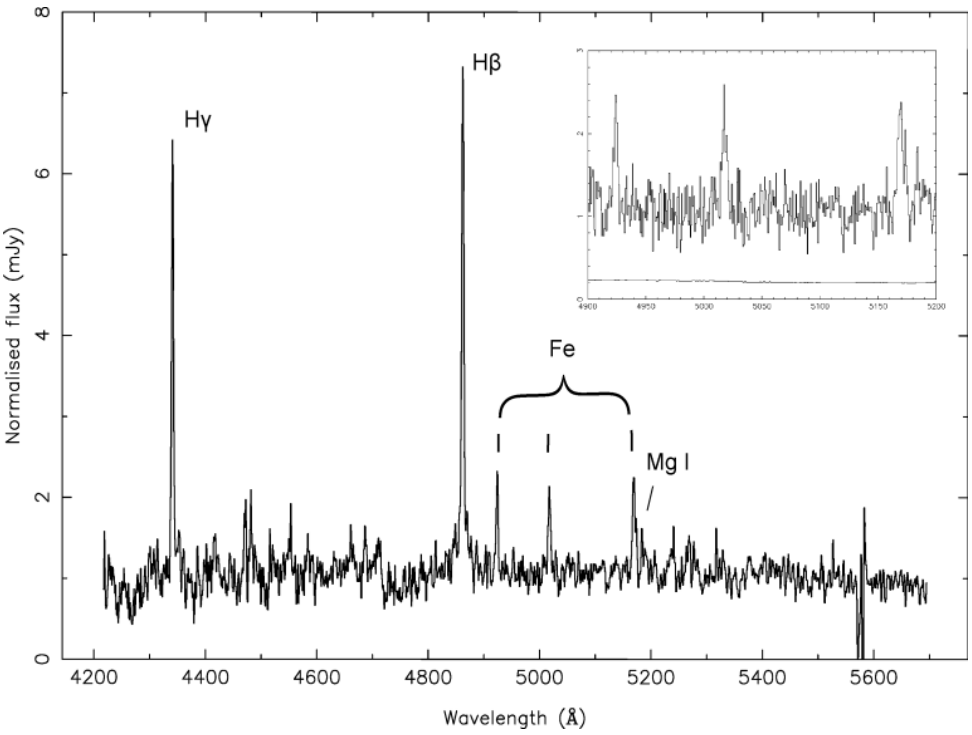


**Figure 4.** Spectrum of the counterpart to EXO 0748−676. This spectrum is an average of thirty-one 900-s-long spectra collected in the phase interval 0.3 and 0.7, corrected for the companion star orbital motion (see Section 3.3). The feature at ∼5577 Å is due to non-perfect subtraction of the night sky O I line at that wavelength. The two prominent emission lines are from H$\gamma$ (4340.465 Å) and H$\beta$ (4861.327 Å). Four weaker lines are marked in the spectrum: the position of the first two is consistent with He I lines, at 4921.929 and 5015.675 Å, but also with Fe II lines at 4923.92 and 5018.44 Å. The third line is consistent with the Fe II line at 5169.03 Å, which favours an interpretation of the first three lines as an Fe II triplet. The fourth weak line can be identified with Mg I at 5183.604 Å. The inset shows a zoom-in of the region of the Fe II triplet and the Mg I line.

**Table 1.** (a) Results from the fitting of individual emission lines in the average spectrum of EXO 0748−676 (see Fig. 4) with a Gaussian function. The wavelength of each line in the rest frame $\lambda_0$ (column 1) is frozen in the fit. The last column of the table indicates the velocity offset of the fitted line centroid with respect to $\lambda_0$. There is evidence for the presence of a narrow spike on the red wing of the Fe II (5169.03) line: we fitted it without masking the spike (superscript '*a*') and masking it (superscript '*b*') (see Section 3.3 for a discussion). (b) Results of the combined multi-Gaussian fit of the three Fe II lines, fitted together forcing the same offset and FWHM in km s$^{-1}$. The spike affecting Fe II (5169.03) is masked. The $v \sin i_{\rm em}$ is measured by artificially broadening arc lines with a grey profile until reaching the FWHM measured for the EXO 0748−676 lines. This accounts for the instrumental resolution profile. The line smearing due to orbital motion during the integration time is also taken into account.

(a)

| $\lambda_0$ (Å) | FWHM (km s$^{-1}$) | Normalization (Å$^2$) | Offset (km s$^{-1}$) |
|---|---|---|---|
| H$\gamma$ (4340.465) | $267 \pm 10$ | $21.9 \pm 0.71$ | $33.1 \pm 8.08$ |
| H$\beta$ (4861.327) | $282 \pm 7$ | $29.9 \pm 0.7$ | $42.5 \pm 6.9$ |
| Fe II (4923.92) | $246 \pm 28$ | $5.6 \pm 0.55$ | $3.5 \pm 12$ |
| Fe II (5018.44) | $366 \pm 50$ | $5.7 \pm 0.61$ | $-50 \pm 21$ |
| Fe II (5169.03)$^a$ | $410 \pm 36$ | $8.4 \pm 0.66$ | $20 \pm 15$ |
| Fe II (5169.03)$^b$ | $311 \pm 41$ | $6.9 \pm 0.77$ | $-15 \pm 11$ |

(b)

| | FWHM (km s$^{-1}$) | $v \sin i_{\rm em}$ (km s$^{-1}$) | Offset (km s$^{-1}$) |
|---|---|---|---|
| Fe II group | $304 \pm 20$ | $255 \pm 22$ | $-15 \pm 11$ |

the averaged spectrum highlights the weak Fe (or He) emission lines.

No absorption lines appear in the averaged spectrum. As for the individual spectra, a cross-correlation of the average spectrum with the standard template spectra does not give a match. Note that we have also constructed an averaged spectrum in the phase intervals 0.8 to 0.2 and 0.9 to 0.1, but we did not detect absorption lines from the non-irradiated face of the companion star.

Table 1 presents the parameters of the best-fitting Gaussian to each line in the averaged spectrum. Each line was fitted for FWHM, normalization and for the offset $\lambda - \lambda_0$ of the line centroid $\lambda$ with respect to the rest-frame wavelength $\lambda_0$. As we corrected the spectra for the orbital motion only, the lines in the average spectrum are still shifted with respect to their rest-frame wavelength by the systemic radial velocity $\gamma$. The wavelength offset of the H$\beta$ and H$\gamma$ lines is consistent on a $2\sigma$ level with the values of $\gamma$ derived from the radial velocity curves (see Section 3.2). The weighted average of the measures of $\gamma$ from the radial velocity curves and from the offsets of the Balmer lines is $\gamma = 43.8 \pm 3.6$ km s$^{-1}$. The offsets of the Fe II lines are not consistent with this value, although they agree with each other on a $3\sigma$ level. In order to understand this difference, we have tested the dependence of the measured line offsets in the averaged spectrum on the choice of $K_{\rm em}$ and $\varphi$ in the orbital motion correction. If the Fe II lines originate in different regions of the companion star, in fact, the two sets of lines will be associated with a different $K_{\rm em}$ and $\varphi$. We found that the offset changes slowly with $K_{\rm em}$, but is sensitive to variations in $\varphi$. The offset of the Fe II lines in the average spectrum is consistent with the measure of $\gamma$ from the Balmer lines if the orbital motion of their source region is shifted in phase by $-0.03 \lesssim \varphi \lesssim -0.05$.

As we previously pointed out, the FWHM of the lines (both H$\gamma$, H$\beta$ and the Fe II group) is not affected by changes in $K_{\rm em}$ of a few tens of km s$^{-1}$ around $\sim$300 km s$^{-1}$. Unlike the offset, it is also not sensitive to changes of a few per cent in $\varphi$. In other words, our measure of the FWHM is not affected by a possible small displacement of the Fe II source region with respect to the source region of the Balmer lines. All the lines in the average spectrum have the same FWHM at a $2\sigma$ level, with the exception of the reddest Fe line, Fe (5169.03 Å), which is significantly broader than Fe (4923.92 Å) at the $>3\sigma$ level. Careful inspection shows a narrow faint emission line on the red end of the 5169.03 Å line (Fig. 4). The presence of this second peak artificially broadens the Gaussian function used to fit the Fe (5169.03 Å) line, as the fitting routine tries to account for both peaks with the same Gaussian. If this narrow peak is masked or fitted with an additional line, the width of Fe (5169.03 Å) becomes consistent within $1\sigma$ with the other lines. It must be noted that a second Gaussian introduced to fit the faint emission near the Fe (5169.03 Å) line helps the fit but is not significant itself (the normalization is approximately equal to the uncertainty on it). After we have verified that the Gaussian fit to the Fe II lines separately provides FWHMs and offsets in agreement with each other, we fitted the triplet together in order to reduce the uncertainty on the parameters. The three Fe lines were forced to have the same FWHM in km s$^{-1}$ and the same velocity offset. The faint emission on the reddest Fe line was masked to avoid artificial broadening. We obtained an FWHM $= 304 \pm 22$ km s$^{-1}$ (reduced $\chi^2 = 0.99$, 994 d.o.f.).

### 3.4 Measuring the intrinsic broadening of the emission lines

The observed FWHM of the emission lines is determined by the intrinsic line width broadened by the instrumental resolution profile and by line smearing produced by the motion of the companion during the integration time of one spectrum. Intrinsic saturation effects can also contribute to the width of the emission lines, significantly affecting strong lines such as the Balmer ones (Osterbrock 1989). On the other hand, if the weak Fe II lines originate on the companion star, their intrinsic width is expected to be dominated by the rotational broadening $v \sin i_{\rm em}$ (Gray 1992). In order to measure the latter from the Fe II triplet, we have artificially smeared and broadened the arc spectra with different values of $v \sin i_{\rm em}$. The $v \sin i_{\rm em}$ resulting in smeared arc lines as broad as the FWHM of the Fe II lines is a measure of the rotational broadening. We proceeded as follows: the phase of each EXO 0748−676 spectrum participating in the average in Fig. 4 was ascribed to one arc spectrum. We smeared the arc spectra by $2\pi T K_{\rm em} \cos(2\pi\phi)/P$, where $T$ is the duration of one exposure (900 s) and $P$ is the orbital period. The smeared arcs were then averaged, each one with the same weight as that of the corresponding (same phase) EXO 0748−676 spectrum in the average of Fig. 4. In this way we have simulated the effect of the smearing due to the orbital motion on the average spectrum. We then broadened the smeared average arc spectrum with a grey profile for different values of $v \sin i_{\rm em}$, measuring each time the resulting FWHM in km s$^{-1}$. We find that the measured FWHM of the Fe II lines corresponds to $v \sin i_{\rm em} = 255 \pm 20$ km s$^{-1}$.

### 3.5 Evidence for Mg I in emission

The average spectrum displays a weak emission line consistent with Mg I at 5183.604 Å. The line was not detectable in the single or trailed spectra, but a fit with a single Gaussian function indicates that the line is significant on a $5\sigma$ level in the average spectrum. Two other Mg I lines, at 5167.321 and 5172.684 Å, belong to the same multiplet with Mg I (5183.604 Å). The position of Mg I (5172.684 Å) is consistent with that of the spike on the

**Table 2.** Best-fitting parameters from the Gaussian fit of the faint emission line identifiable with Mg I (5183.604 Å) in the average spectrum (see Fig. 4). The last column reports the intrinsic line width $v \sin i_{\rm em}$, measured as for the Fe II lines (see caption to Table 1).

| $\lambda_0$ (Å) | FWHM ($\rm km\,s^{-1}$) | Normalization (Å$^2$) | Offset ($\rm km\,s^{-1}$) | $v \sin i_{\rm em}$ ($\rm km\,s^{-1}$) |
|---|---|---|---|---|
| Mg I (5183.604) | $172 \pm 39$ | $2.2 \pm 0.4$ | $8 \pm 16$ | $98 \pm 39$ |

red wing of Fe II (5169.03 Å; see Fig. 4), although the detection of the latter is not statistically significant when the prominent Fe II line is included in the fit. Mg I (5167.321 Å) could be present but it cannot be resolved from Fe II (5169.03 Å). The FWHM of the Mg I (5183.604 Å) line is $172 \pm 39$ $\rm km\,s^{-1}$ (see Table 2), which corresponds to an intrinsic width of $v \sin i_{\rm em} = 98 \pm 39$ $\rm km\,s^{-1}$ (a measure as we did for the Fe II triplet in Section 3.4). This value is smaller than what we obtained from the Fe II triplet.

### 3.6 Doppler tomography

We employed emission-line Doppler tomography to map the observed emission features. Here we used the modulation Doppler tomography method of Steeghs (2003), using the same code as was employed in the Bassa et al. (2009) study. The observed spectra were first phase binned using 30 orbital bins. The underlying continuum was subtracted using a polynomial fit to line-free regions. In Fig. 5 we show the resulting tomograms for the H$\beta$ line and the two Fe II lines at 4923.92 and 5169.03 Å. The H$\gamma$ line reconstructions were effectively identical to H$\beta$ and we compare the two Fe II lines given their apparent difference in intrinsic width. All emission-line reconstructions are consistent with line emission from a region near the mass donor star with no evidence for any extended emission from a residual accretion disc or stream. We find that the line flux is strongly modulated, as expected for an origin on the irradiated face of the companion, and in phase with the observed continuum modulation. Good fits are achieved close to a reduced $\chi^2$ of 1.

The Doppler maps confirm the key attributes we derived in the previous sections using Gaussian fitting. We find that the radial velocity amplitude of the emission ranges from 300 to 350 $\rm km\,s^{-1}$, consistent with the $K_{\rm em}$ values from Section 3.3 as well as past estimates of $K_2$. We show in Fig. 5 the expected location of the donor Roche lobe and gas stream using a mass ratio of $q = 0.25$ (consistent with the NS mass range favoured by Özel 2006 and Muñoz-Darias et al. 2009; see also Bassa et al. 2009) and $K_2 = 410\,\rm km\,s^{-1}$. The latter is the lower limit to $K_2$ obtained by Bassa et al. (2009), which is a more stringent constraint compared to that we derived in the previous sections (see the discussion in Section 5). Again, the line at 5169.03 Å appears somewhat anomalous with a significantly more extended emission distribution, reflecting its observed width. Furthermore, the centre of the emission is shifted slightly off the Roche lobe, consistent with the apparent phase shift mentioned previously.

In summary, our Doppler tomograms confirm that the narrow emission lines are consistent with an origin on the irradiated face of the mass donor star, with the exception of the emission feature at 5169.03 Å which is both extended and shifted with respect to the other lines. This is in agreement with the broadening effect observed in the Gaussian fitting of 5169.03 Å (Section 3.3). We will discuss this further in Section 5.

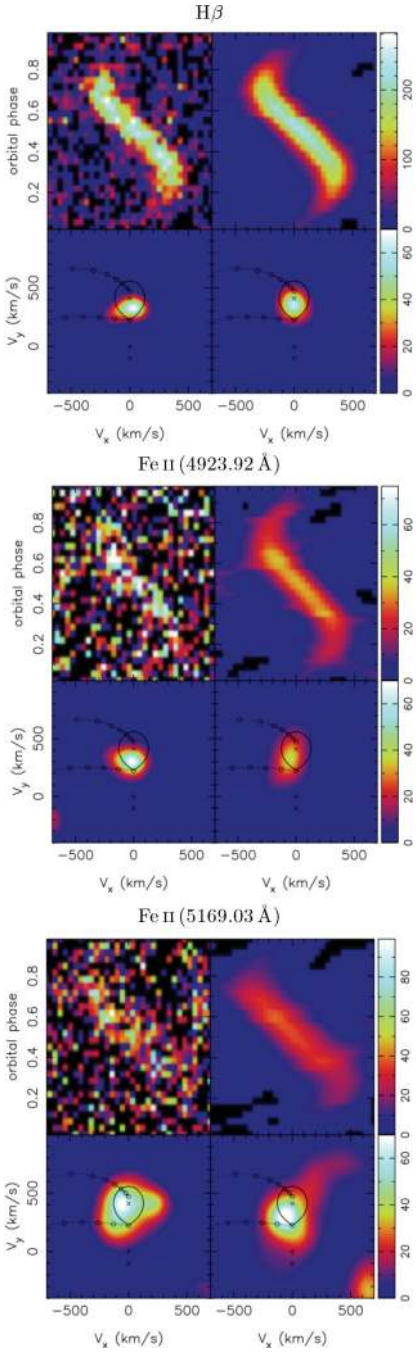


**Figure 5.** Tomographic reconstructions for the H$\beta$ and Fe II lines at 4923.92 and 5169.03 Å. The top-left panel in each case shows the observed line profile as a function of the orbital phase while the top-right panel shows the reconstructed data from the converged maximum entropy solution. The bottom panels show the Doppler maps resolving the emission of each line in a $V_X$–$V_Y$ plane. The constant and the phase-dependent contribution to the flux are shown in the left and right quadrants, respectively (see Steeghs 2003). The colour scale indicates the fractional amplitude of the variable map in per cent. A Roche lobe model and ballistic stream trajectory is plotted for an assumed system mass ratio of $q = 0.25$ and radial velocity semi-amplitude of the companion star $K_2 = 410\,\rm km\,s^{-1}$.

## 4 SUMMARY OF THE RESULTS

The results presented in the previous sections can be summarized as follows.

(i) The $g'$-band light curve of the source spans a range of 1 mag. The profile is variable, but the errors on the individual magnitudes are large: significant variability at a $3\sigma$ level is detected within the phase interval of 0.007 starting from phase 0.349, with an amplitude of $0.35 \pm 0.08$ mag (Fig. 2, top panel). The morphology of the light curve in the $g'$ band is similar to that of the $r'$-band light curve reported by Bassa et al. (2009), albeit the latter is not variable.

(ii) The spectra show emission lines from H$\beta$ and H$\gamma$ and three weaker lines consistent with Fe II (4923.92 Å) or He I (4921.929 Å), Fe II (5018.44 Å) or He I (5015.675 Å) and Fe II (5169.03 Å). Since there is no He I line at the position of the last weak emission feature, we favour an Fe II group interpretation. A weak emission line consistent with Mg I (5183.604) is also detected at a $5\sigma$ level in the average spectrum.

(iii) The orbital motion displayed by the emission lines is consistent with them originating close to the surface of the companion star facing the NS. The phasing of the continuum variation is in sync with the strong orbital modulation of the emission-line strength, as expected if both are mainly produced by the irradiated companion. Evidence of an irradiated companion star was previously found, both during the X-ray outburst phase (Pearson et al. 2006; Muñoz-Darias et al. 2009) and at the beginning of the quiescent period (Bassa et al. 2009).

(iv) The broad disc component at the base of the emission lines that was detected in the spectra from Bassa et al. (2009) is not detected here. There is no evidence for an accretion disc either from the line profiles or from the Doppler tomography.

(v) The fitting of the radial velocity curves of the H$\gamma$ and H$\beta$ lines provides $1\sigma$ consistent measures of the radial velocity amplitude of the emission lines $K_{\rm em}$, whose weighted average is $308.5 \pm 3.9\,{\rm km\,s^{-1}}$. The minimum width of the emission lines in the average spectrum is obtained with an orbital-motion correction with $K_{\rm em} \sim 300\,{\rm km\,s^{-1}}$, in agreement with the radial velocity curves estimate. This measurement provides a lower limit on the radial velocity semi-amplitude of the companion star $K_2$, which is fully consistent with the results of Muñoz-Darias et al. (2009). A more stringent lower limit on $K_2$ is reported by Bassa et al. (2009) (see discussion in Section 5).

(vi) The systemic radial velocity $\gamma$ was measured from the radial velocity curve traced by the H$\gamma$ and H$\beta$ lines and from the wavelength offset of the same lines in the orbital-motion subtracted averaged spectrum. The resulting values of $\gamma$ are in agreement within $2\sigma$, their weighted average being $43.8 \pm 3.6\,{\rm km\,s^{-1}}$. The offset of the Fe II triplet in the average spectrum, instead, is inconsistent with this value of $\gamma$. A phase shift of $-0.03/-0.05$ of the source region of the Fe II lines with respect to the binary axis can account for this discrepancy (see Section 5). The Doppler maps also show that the emission of the Fe II lines is shifted, particularly for the one at 5169.03 Å. Our measure of the systemic radial velocity is in agreement with the work of Muñoz-Darias et al. (2009), but is more than $5\sigma$ apart from the value obtained by Bassa et al. (2009), $\gamma = 78.6 \pm 3.9\,{\rm km\,s^{-1}}$. Even taking into account that the value of $\gamma$ is affected by the accuracy of the wavelength calibration (0.023 Å in Bassa et al. 2009 and 0.1 Å for our data), the two measurements differ by more than $4\sigma$. Similar mismatches using VLT data are not unprecedented (see Orosz et al. 2011).

(vii) With the exception of the weak Mg I, the emission lines are very broad. The FWHM of the Fe II lines indicates a $v \sin i_{\rm em} = 255 \pm 22\,{\rm km\,s^{-1}}$, if the broadening results from the rotation of the companion star alone. The Mg I (5183.604 Å) line instead provides a much lower $v \sin i_{\rm em}$ of $98 \pm 39\,{\rm km\,s^{-1}}$.

## 5 DISCUSSION

Using medium-resolution VLT FORS2 spectra of EXO 0748−676, ranging from 4222 to 5701 Å, we found emission lines indicating that the companion star is still heated by irradiation, as was observed soon after the onset of the quiescent phase (Bassa et al. 2009). We detected H$\gamma$, H$\beta$ and a set of Fe II lines, which is unusual but not unprecedented in LMXBs (Marsh, Robinson & Wood 1994). We also detect a faint Mg I line. The source of the irradiation is most likely the X-rays associated with the cooling compact object (Degenaar et al. 2009). The slow rate of the NS cooling that has been observed in EXO 0748−676 with *XMM–Newton*, *Chandra* and *Swift* (Degenaar et al. 2011; Díaz Trigo et al. 2011) is in agreement with the fact that the companion star is still significantly irradiated, after more than 1 yr of quiescence.

The $g'$-band light curve of EXO 0748−676 shows evidence for variability between different orbits, in the phase interval of 0.007 starting from phase 0.349. The variability amplitude is $0.35 \pm 0.08$ mag. This implies a change in the flux heating the companion star, which could potentially be due to a change in a pulsar wind (see below) or to variability in the X-ray radiation, although the latter is hard to explain given the small variations observed in the X-rays (Degenaar et al. 2011; Díaz Trigo et al. 2011). Furthermore, theoretically one does not expect the X-ray flux of the glowing cooling NS to vary on short time-scales (Brown, Bildsten & Chang 2002). A comparison with the *R*-band light curve presented in Bassa et al. (2009) shows that the morphology of the light curves is similar, albeit the $g'$-band one is variable.

Although we cannot rule out a disc contribution to the optical continuum, the non-detection of disc line emission is unusual in comparison with typical observations of quiescent LMXBs (e.g. Marsh et al. 1994; Torres et al. 2002). The disc-instability model that can explain the short outburst of typical X-ray transients (Smak 1971; Dubus, Hameury & Lasota 2001) predicts that the disc is present even during quiescence and that an outburst is triggered by a sudden rise of viscosity. The lack of disc lines in EXO 0748−676 suggests instead that the mass transfer has dramatically dropped and might have even stopped since the observations performed by Bassa et al. (2009) at the beginning of the quiescent phase. On the other hand, the disc-instability model might not apply to the case of EXO 0748−676 as it cannot easily explain the 20-yr-long outburst that the source underwent. The trigger of tens-of-years-long outbursts is not well understood and might have to do with variations in the envelope of the companion star, rather than with instabilities of an accretion disc (Remillard & McClintock 2006).

In an attempt to obtain constraints on the NS mass from the emission lines, we determined the rotational velocity obtained from the FWHM of the Fe II triplet observed in the spectra. If those lines are produced on the companion star surface, their width is expected to be dominated by the effect of rotational broadening $v \sin i_{\rm em}$ (Gray 1992). As also emerged from the tomographic reconstructions, the line emission does not arise from the full inner hemisphere of the companion star, but concentrates close to L1 point. For this reason, $v \sin i_{\rm em}$ obtained from the Fe II lines would represent a lower limit to the projected spin velocity of the star $v \sin i$. Due to the shift between the centre of light of the Fe emission lines and the centre of mass of the companion, the radial velocity semi-amplitude of the emission lines $K_{\rm em}$ also provides only a lower limit to $K_D$. The combination of the lower limits on $K_D$ and $v \sin i$ provides in turn a lower limit on the NS mass. From the radial velocity curves and our average spectrum, we measured $K_2 \gtrsim 308.5 \pm 3.9\,{\rm km\,s^{-1}}$ (see Sections 3.2 and 3.3). From the Doppler maps (which are not

influenced by asymmetries in the line profiles; see Bassa et al. 2009), we obtain a higher limit, $K_2 \gtrsim 355\,\mathrm{km\,s^{-1}}$. An even more stringent limit is provided in Bassa et al. (2009), $K_2 \gtrsim 405\,\mathrm{km\,s^{-1}}$. This was obtained from Doppler tomography of the H$\alpha$ line, which is expected to form closer to the centre of mass of the companion star with respect to higher ionization potential lines such as H$\beta$ and H$\gamma$, providing a radial velocity closer to $K_D$ (e.g. Harlaftis et al. 1999; Unda-Sanzana, Marsh & Morales-Rueda 2006).

The constraints on the mass of the NS in EXO 0748−676 that can be obtained combining the results of Bassa et al. (2009) with our measure of $v \sin i_{\mathrm{em}}$ show that, if the width of the Fe lines in our spectra is indeed setting a lower limit to $v \sin i$, then the mass of the compact object in EXO 0748−676 should be $\gtrsim$3.5 $\mathrm{M}_\odot$. This is more than the value of $\sim$3 $\mathrm{M}_\odot$ which is considered to be an upper bound to the mass of an NS. A BH interpretation would be in conflict with the detection of thermonuclear X-ray bursts from the source, which establishes that the compact object is an NS (Gottwald et al. 1986). Given the fact that a bursting BH or a 3.5 $\mathrm{M}_\odot$ NS would be against theories about those objects, we have investigated possible scenarios to solve this incongruity.

Our mass constraint is based on the assumption that the width of the Fe lines provides a measure of the projected rotational velocity of the companion star $v \sin i$, but that might not be the case. An asymmetric irradiation of the companion due e.g. to the shadowing of a residual accretion disc could induce currents in the atmosphere trying to re-distribute the heat (Kirbiyik 1982; Wolff et al. 2002). The velocity of the current would add to the width of the emission lines. Nevertheless, this velocity has to be of the order of the total line broadening in order to give a significant contribution, i.e. a few hundreds $\mathrm{km\,s^{-1}}$. This is more than the sound speed on the surface of a late-type star (Frank, King & Raine 2002).

Another possibility is that the Balmer lines, originating closer to the companion star surface, are broadened by saturation effects (Osterbrock 1989), while the Fe II triplet, slightly phase shifted, is produced in a stream of residual accreting matter whose velocity causes the observed FWHM. This interpretation requires a little fine-tuning of two broadening effects and it does not fit well with the lack of any evidence for an accretion disc.

The large width of the Fe lines could also be due to a blend with unresolved lines of other atomic species. This is suggested by the detection of a faint ($5\sigma$ significance) line consistent with Mg I at 5183.604 Å. As mentioned in Section 3.5, the latter belongs to a Mg I multiplet including lines at 5167.321 and 5172.684 Å, both very close to the position of the reddest detected Fe II line. Mg I (5172.684 Å) might be identified with the peak next to Fe II (5169.03 Å) that we have masked when measuring the FWHM of the Fe II line. The peak is not significant in the average spectrum, but the anomalous extension and shift of Fe II (5169.03 Å) in the Doppler maps suggest that this narrow feature might be real and present in all the spectra, altering the look of the line in the tomographic reconstruction. On the other hand, Mg I (5167.321 Å) could be present, but it is not resolved from Fe II (5169.03 Å). While a blend with Mg I can explain the width of Fe II (5169.03 Å), a blend with He I can broaden the other two lines of the Fe II triplet. As in the 'stream' scenario, the FWHM of H$\beta$ and H$\gamma$ would instead be determined by saturation effects. The downside of this sketch is that it requires some fine-tuning of the width and intensity of the lines of different species in order to produce consistent FWHM and offsets among the three Fe II lines. Other lines from Mg I and He I (at 4387.928 and 4471.68 Å) that are within the wavelength coverage of our observation are not detected, so we have to meet the further requirement that only the lines that overlap with Fe II are strong enough to be observed. Although the Mg I (5183.604 Å) detection supports this scenario, we cannot confirm it or rule it out with the resolution and signal-to-noise ratio of our observations.

For this reason, we have considered another possible situation, where the lines are produced in a wind of matter evaporating from the companion star, e.g. due to the action of a pulsar wind and/or the X-ray heating. The emission lines, originating in the wind of evaporated material, are broadened due to the wind velocity. The Balmer lines, produced closer to the companion star surface, display the orbital motion of the irradiated secondary, while the Fe II, rising from further out in the wind, displays a slight phase delay in the orbital motion as the evaporated material starts to trail the companion star as it moves outwards due to angular momentum conservation. The evaporation of material could also explain the lack of evidence for emission lines from an accretion disc, as it would quench the accretion. Moreover, the presence of a pulsar wind in addition to the X-ray heating might be responsible for the observed variability in the $g'$-band light curve, which is possible but rather difficult to produce in terms of variability of the X-ray flux. At last, this 'Black-widow-like' scenario is consistent with the extended distribution of the line emission in the Doppler maps. The weak point of this outline is that it may be difficult to produce Mg I (5183.604 Å), which is narrower than the other lines. The weakness of the line did not allow the production of Doppler maps to verify if the source region of this feature is narrow or extended and if it is the same as the Balmer or Fe II lines. Moreover, it has to be noted that the pulsar in quiescence has not been found in the radio waveband (M. Burgay, private communication).

## 6 CONCLUSIONS

We performed phase-resolved medium-resolution optical spectroscopy with VLT/FORS2 on the eclipsing LMXB EXO 0748−676, one year and two months after it returned to quiescence. We found evidence for variability in the $g'$-band light curve and that the spectra only present emission lines coming from the region close to the companion star, with no line contribution from a disc. This is unusual compared with typical X-ray transients and could be related to the mechanism that triggers long-duration outbursts such as those displayed by the source, which is not yet understood.

The $g'$-band variability can be explained either by a varying X-ray flux or by a variable pulsar wind. X-ray observations show little variations in the flux, as expected from a cooling NS.

The H$\beta$, H$\gamma$ and Fe II emission lines in the average spectrum are remarkably broad. Their FWHM is not likely to be dominated by rotational broadening alone as this would lead to a compact object mass inconsistent with an NS. The width of the lines can be explained with bulk gas motion, e.g. the lines could be produced in a wind of material evaporated from the companion star envelope due to X-ray heating, possibly in combination with a pulsar wind. It is also possible that some of the lines are blends of unresolved features. Despite extensive efforts to search for spectral features using multiple methods, we detect no absorption features from the mass donor star. Deeper observations with better resolution might allow us to resolve blends and detect more emission lines that could provide a reliably lower limit to the companion star rotational broadening and, in turn, to the NS mass. Moreover, there is still the chance to detect absorption lines from the non-irradiated face of the companion star, which would finally provide a mass estimate for this elusive NS.

## ACKNOWLEDGMENTS

PGJ acknowledges support from a VIDI grant from the Netherlands Organisation for Scientific Research. Tom Marsh is thanked for developing and sharing his packages PAMELA and MOLLY.

## REFERENCES

Bassa C. G., Jonker P. G., Steeghs D., Torres M. A. P., 2009, MNRAS, 399, 2055
Brown E. F., Bildsten L., Chang P., 2002, ApJ, 574, 920
Chakrabarty D., 2005, in Burderi L., Antonelli L. A., D'Antona F., di Salvo T., Israel G. L., Piersanti L., Tornambè A., Straniero O., eds, AIP Conf. Ser. Vol. 797, Interacting Binaries: Accretion, Evolution, and Outcomes. Springer Verlag, New York, p. 71
Charles P. A., Coe M. J., 2006, in Lewin W., van der Klis M., eds, Cambridge Astrophys. Ser. Vol. 39, Compact Stellar X-Ray Sources. Cambridge Univ. Press, Cambridge, p. 215
Degenaar N. et al., 2009, MNRAS, 396, L26
Degenaar N. et al., 2011, MNRAS, 412, 1409
Díaz Trigo M., Boirin L., Costantini E., Méndez M., Parmar A., 2011, A&A, 528, A150
Dubus G., Hameury J.-M., Lasota J.-P., 2001, A&A, 373, 251
Frank J., King A., Raine D. J., eds, 2002, Accretion Power in Astrophysics, 3rd edn. Cambridge Univ. Press, Cambridge
Gottwald M., Haberl F., Parmar A. N., White N. E., 1986, ApJ, 308, 213
Gray D. F., 1992, The Observation and Analysis of Stellar Photospheres, Cambridge Astrophys. Ser. Vol. 20. Cambridge Univ. Press, Cambridge
Harlaftis E., Collier S., Horne K., Filippenko A. V., 1999, A&A, 341, 491
Horne K., 1985, MNRAS, 213, 129
Horne K., 1986, PASP, 98, 609
Hynes R. I., Jones E. D., 2009, ApJ, 697, L14
Kirbiyik H., 1982, MNRAS, 200, 907
Lattimer J. M., Prakash M., 2001, ApJ, 550, 426
Marsh T. R., Robinson E. L., Wood J. H., 1994, MNRAS, 266, 137
Moore C. E., 1972, A Multiplet Table of Astrophysical Interest – Part 1: Table of Multiplets; Part 2: Finding List of All Lines in the Table of Multiplets. Princeton Univ. Press, Princeton, NJ
Muñoz-Darias T., Casares J., O'brien K., Steeghs D., Martínez-Pais I. G., Cornelisse R., Charles P. A., 2009, MNRAS, 394, L136
Orosz J. A., Steiner J. F., McClintock J. E., Torres M. A. P., Remillard R. A., Bailyn C. D., Miller J. M., 2011, ApJ, 730, 75
Osterbrock D. E., 1989, Astrophysics of Gaseous Nebulae and Active Galactic Nuclei. University Science Books, Mill Valley, CA, p. 422
Osterbrock D. E., Fulbright J. P., Martel A. R., Keane M. J., Trager S. C., Basri G., 1996, PASP, 108, 277
Özel F., 2006, Nat, 441, 1115
Parmar A. N., White N. E., Giommi P., Haberl F., 1985, IAU Circ.4039
Parmar A. N., White N. E., Giommi P., Gottwald M., 1986, ApJ, 308, 199
Pearson K. J. et al., 2006, ApJ, 648, 1169
Remillard R. A., McClintock J. E., 2006, ARA&A, 44, 49
Smak J., 1971, Acta Astron., 21, 15
Steeghs D., 2003, MNRAS, 344, 448
Stetson P. B., 1987, PASP, 99, 191
Torres M. A. P., Casares J., Martínez-Pais I. G., Charles P. A., 2002, MNRAS, 334, 233
Torres M. A. P., Jonker P. G., Steeghs D., Seth A. C., 2008, Astron. Telegram, 1817, 1
Unda Sanzana E., Marsh T. R., Morales-Rueda L., 2006, MNRAS, 369, 805
van Paradijs J., McClintock J. E., 1995, in Lewin W. H. G., van Paradijs J., van den Heuvel E. P. J., eds, Cambridge Astrophys. Ser. Vol. 26, X-Ray Binaries. Cambridge Univ. Press, Cambridge, p. 58
Wade R. A., Horne K., 1988, ApJ, 324, 411
Wijnands R., Miller J. M., Markwardt C., Lewin W. H. G., van der Klis M., 2001, ApJ, 560, L159
Wolff M. T., Hertz P., Wood K. S., Ray P. S., Bandyopadhyay R. M., 2002, ApJ, 575, 384
Wolff M., Ray P., Wood K., Wijnands R., 2008a, Astron. Telegram, 1812, 1
Wolff M. T., Ray P. S., Wood K. S., 2008b, Astron. Telegram, 1736, 1
Wolff M. T., Ray P. S., Wood K. S., Hertz P. L., 2009, ApJS, 183, 156

This paper has been typeset from a TEX/LATEX file prepared by the author.